Supporting Information

Electrocatalytic reduction of 4-nitrophenol over Ni-MOF/NF: understanding the self-enrichment effect of H-bond

Huaiquan Zhao, Xuliang Pang, Yifei Huang, Yajie Bai, Jinrui Ding, Hongye Bai*, Weiqiang Fan*

School of Chemistry and Chemical Engineering, Jiangsu University, Zhenjiang 212013, P. R. China.

**Emails: bhy198412@163.com, fwq4993329@yahoo.com*

1. EXPERIMENTAL SECTION

1.1. Chemicals and reagents

Nickel nitrate hexahydrate ($Ni(NO_3)_2 \cdot 6H_2O$), 1,3,5-trimesic acid (BTC), tributylmethylammonium methyl sulfat (MTBS), N,N-dimethylformamide (DMF), 4-nitrophenol (4-NP), 4-aminophenol (4-AP), potassium hydroxide (KOH), and sodium borohydride ($NaBH_4$) were purchased from Sinopharm Chemical Reagent Co., Ltd in China. Deionized water was used throughout the experiment. The thickness of nickel foam (NF) was 1.0 mm.

1.2 Synthesis of Ni-MOF/NF

Electrochemical deposition was carried out in a three-electrode system, with a piece of NF (1×2 cm^{-2}) as the working electrode, Ag/AgCl electrode as the reference electrode, and platinum wire as the counter electrode. 50 mL DMF solution with 0.045 M $Ni(NO_3)_2 \cdot 6H_2O$, 0.1 M BTC and 0.1 M MTBS was used as the electrolyte.[1] Electrochemical deposition was operated at -1.5 V vs. Ag/AgCl (Figure S1). The obtained samples were washed by water and ethanol, and then dried in an oven at 60 ℃. The amount of Ni-MOF decorated on NF was controlled by deposition time, and the deposition times were 200 s, 400 s, 600 s, and 800 s, and the corresponding samples were marked as Ni-MOF-200/NF, Ni-MOF-400/NF, Ni-MOF-600/NF, and Ni-MOF-800/NF.

1.3. Characterization

The surface morphology of samples was studied by scanning electron microscope (SEM, Hitachi S-4800). The crystal structure was further characterized by X-ray diffraction (XRD, Bruker D8 ADVANCE X-ray diffractometer with Cu-Ka radiation source). Fourier transform infrared spectroscopy (FT-IR, Nexus 470, Thermo Electron Corporation) was used to study the functional groups of samples. X-ray photoelectron spectroscopy (XPS, Thermos Fisher Scientific, Escalab 250Xi, Al Ka) was used to investigate the composition and valence state of elements. Qualitative and quantitative research of reaction was carried out by the ultraviolet-visible (UV-vis) absorption spectrometer (Agilent Technologies Cary 8454 UV-Vis).

1.4. Electrochemical experiments

All the electrochemical tests were carried out by electrochemical workstation (CHI 660E) in a three-electrode system, where Ni-MOF/NF, Ag/AgCl electrode and platinum wire were used as the working electrode, reference electrode and counter electrode, respectively. The linear sweep voltammograms (LSV) was measured in a

voltage range of 0−-1.2 V vs. Ag/AgCl with a sweep rate of 5 $mV \cdot s^{-1}$. Electrochemical reduction of 4-NP was measured in 50 mL KOH aqueous solution (0.1 M) with 0.5 mM 4-NP.

1.5. Product analysis

400 μL reaction solution was diluted with 2 mL distilled water, and the diluted solution was transferred to a quartz cell and further measured by the UV-vis absorption spectrometer. 4-NP performs an obvious UV-vis absorption peak at 400 nm, and the alternation of intensity was monitored. The quantitative analysis of related products was determined by the standard curve of absorption peak at 400 nm.

The calculation formulas of reaction rate (v) and conversion rate are as follows:

$$v = \frac{(C_0 - C) \cdot V}{t \cdot m}$$

$$\text{conversion rate (\%)} = (1 - \frac{C}{C_0}) \times 100\ \%$$

Where v is the reaction rate, C_0 is the initial concentration of reactants, C is the concentration of reactants after reaction, V is the volume of reaction solution, t is the reaction time, and m is the mass of catalyst.

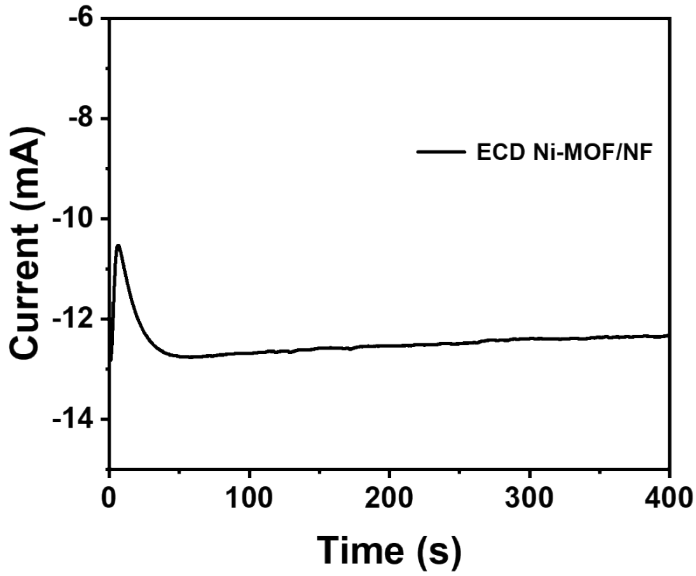

Fig. S1. I-t curve for electrochemical deposition of Ni-MOF/NF.

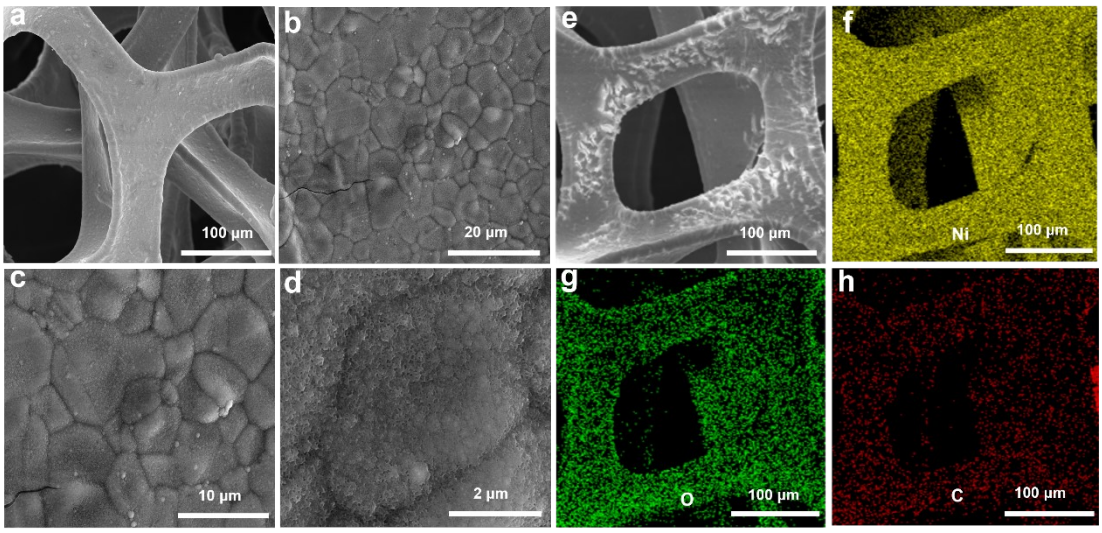

Fig. S2. (a-d) SEM images and (e-h) EDS elemental mapping images of Ni-MOF/NF.

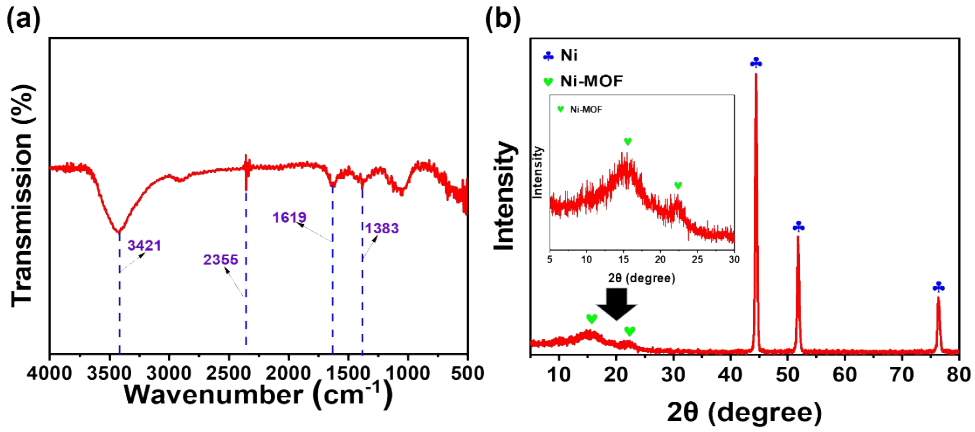

Fig. S3. (a) FT-IR spectroscopy and (b) XRD pattern of Ni-MOF/NF.

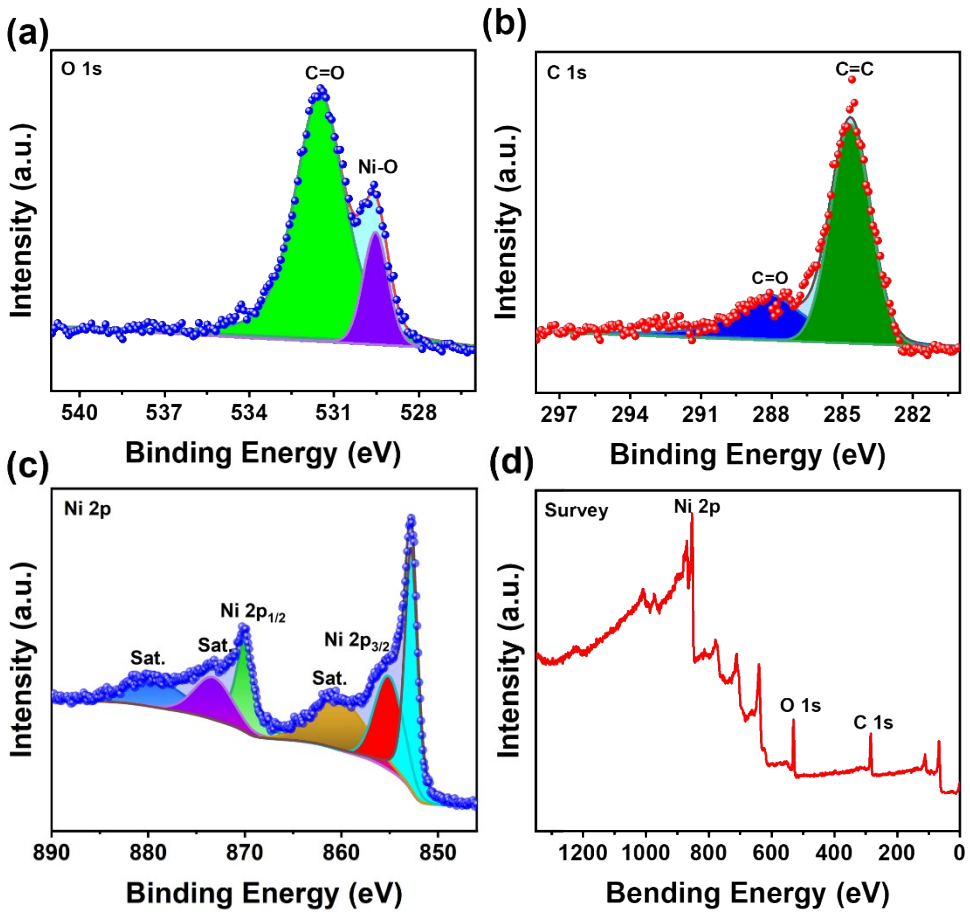

Fig. S4. XPS spectra of (a) O 1s, (b) C 1s, (c) Ni 2p and (d) survey for Ni-MOF/NF.

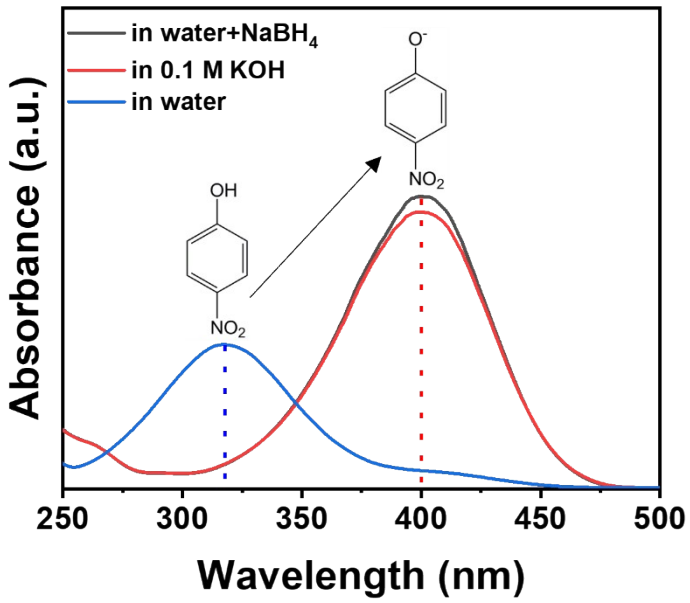

Fig. S5. UV-vis absorption spectra of 4-NP in pure water, 2.5 mM $NaBH_4$ solution and 0.1 M KOH (pH 13) solution, respectively.

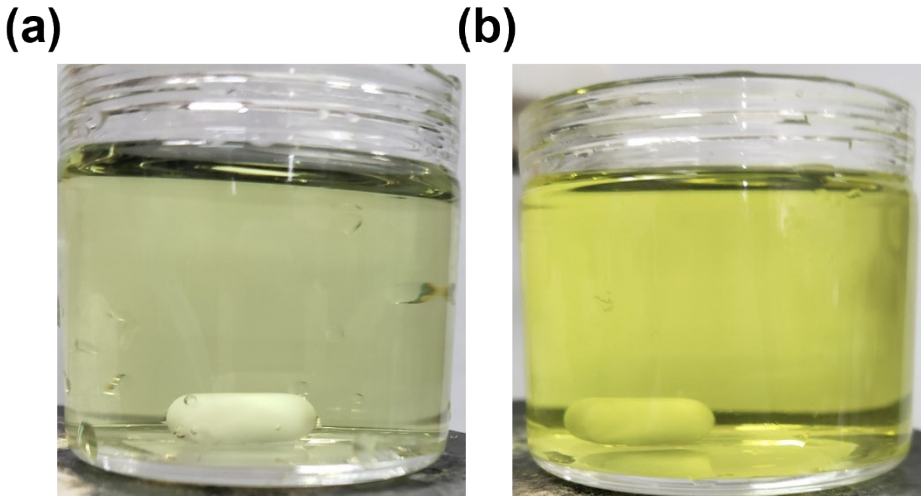

Fig. S6. 4-NP in pure water before (a) and after (b) adding $NaBH_4$.

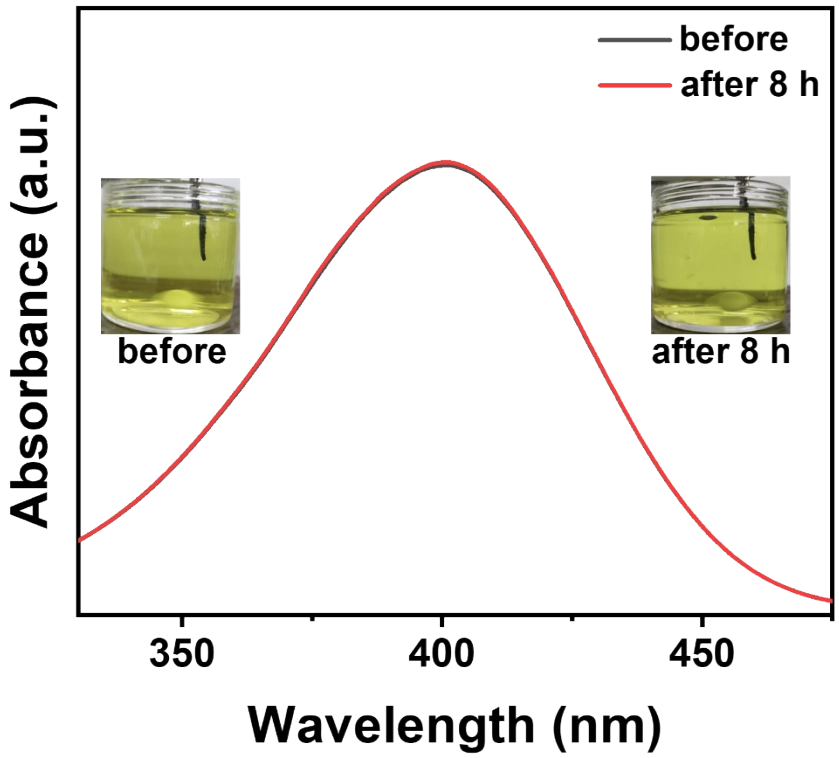

Fig. S7. UV-vis absorption spectra of 4-NP and product after 8 h without electric field.

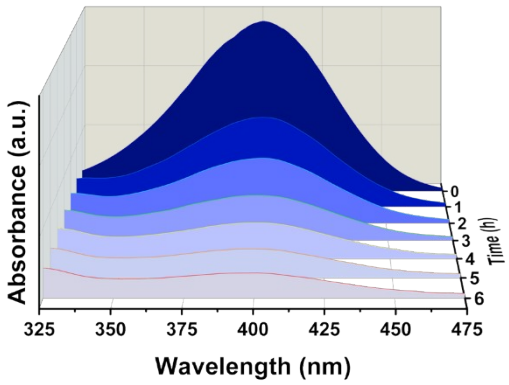

Fig. S8. UV-vis absorption spectra of 4-NP (0.5 mM, 50 mL) at different reaction time (-1.0 V vs. Ag/AgCl).

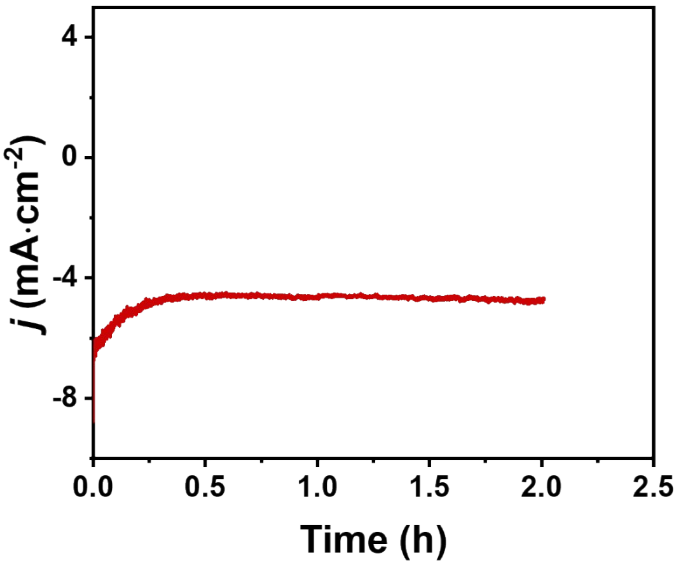

Fig. S9. Current–time during constant-potential electrolysis at -1.0 V vs Ag/AgCl.

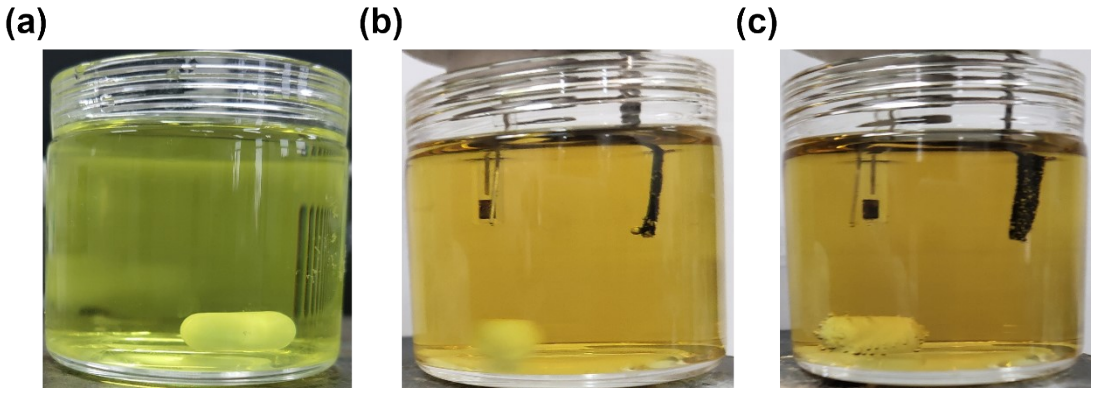

Fig. S10. Color change of 4-NP (in 0.1 M KOH) before (a), after 1 h (b) and 2 h (c) reaction during constant-potential electrolysis at -1. 0 V vs Ag/AgCl.

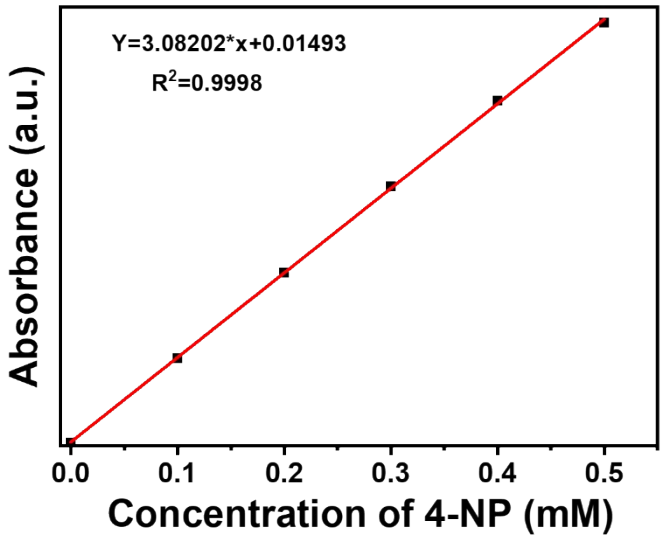

Fig. S11. Standardized curve of UV absorption intensity with concentration.

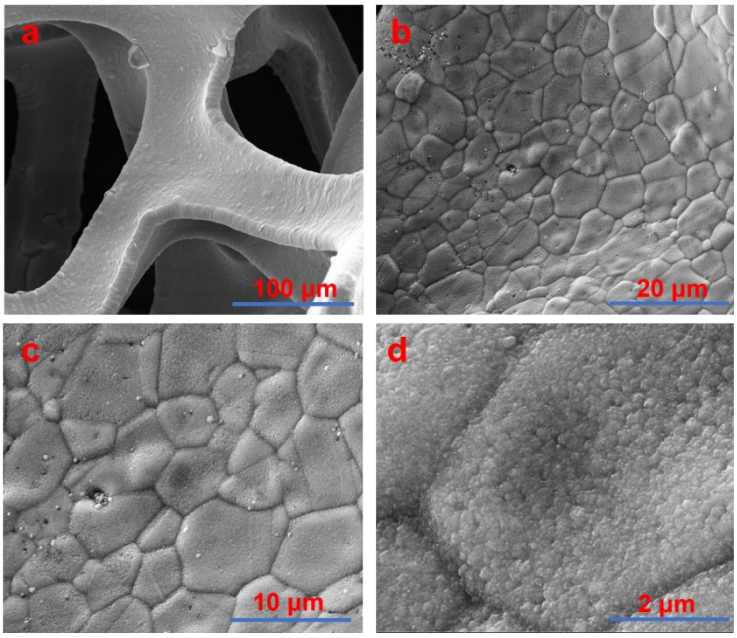

Fig. S12. (a-d) SEM images of Ni-MOF/NF after reaction during constant-potential electrolysis at -1.0 V vs Ag/AgCl.

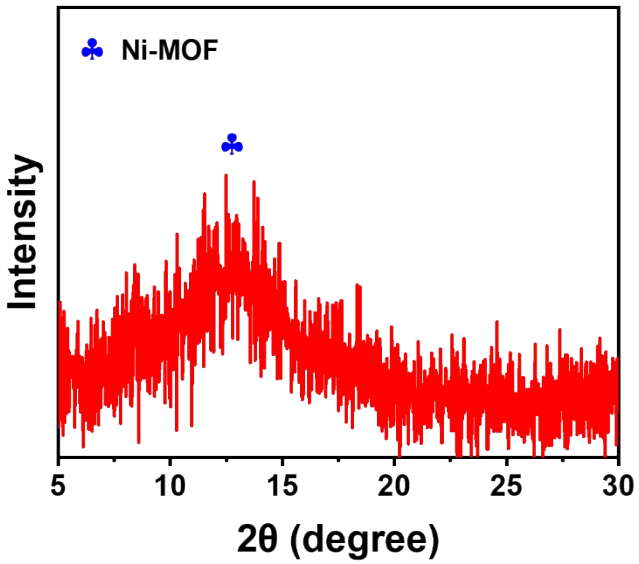

Fig. S13. XRD pattern of Ni-MOF/NF after reduction of 4-NP (2 h, -1.0 V vs. Ag/AgCl).

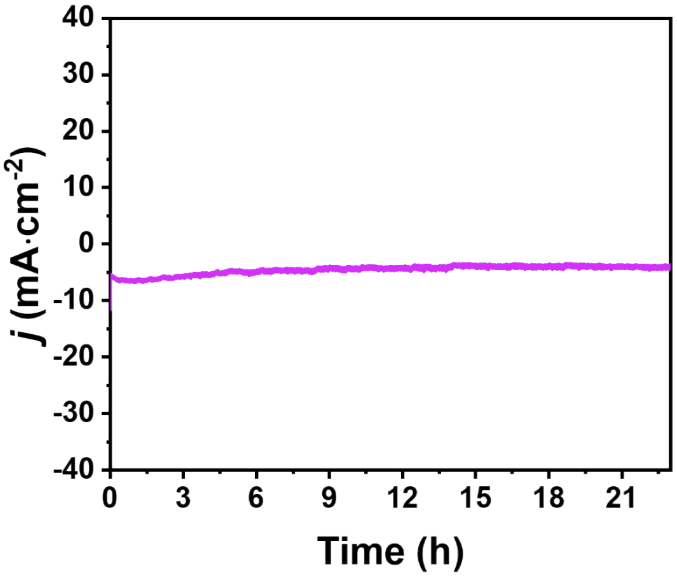

Fig. S14. Current–time during constant-potential electrolysis at -1.0 V vs Ag/AgCl.

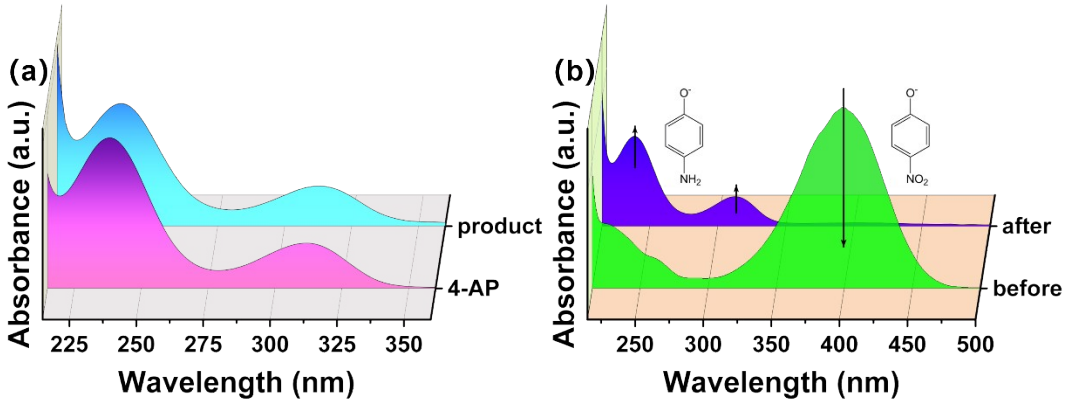

Fig. S15. (a) UV-vis absorption spectra of standard 4-AP sample and product in 0.1 M KOH. (b) UV-vis absorption spectra of reactant and reductive product (-1.2 V vs. Ag/AgCl, initial concentration of 4-NP: 0.5 mM).

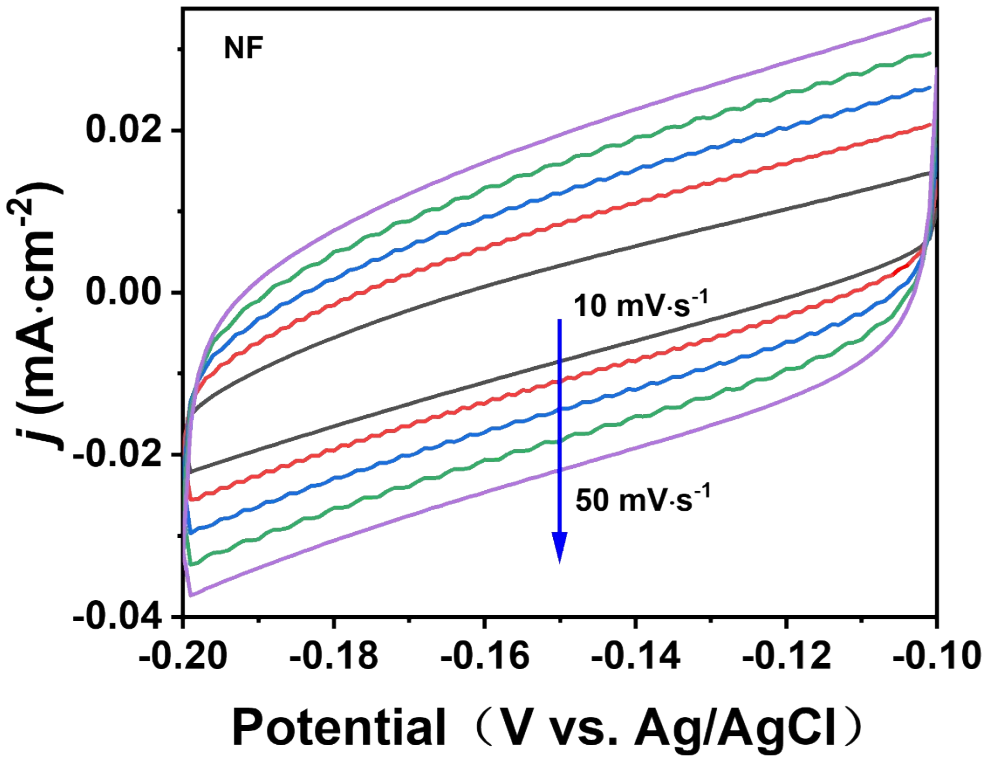

Fig. S16. CV curves of NF at different scan rates (0.5 mM 4-NP).

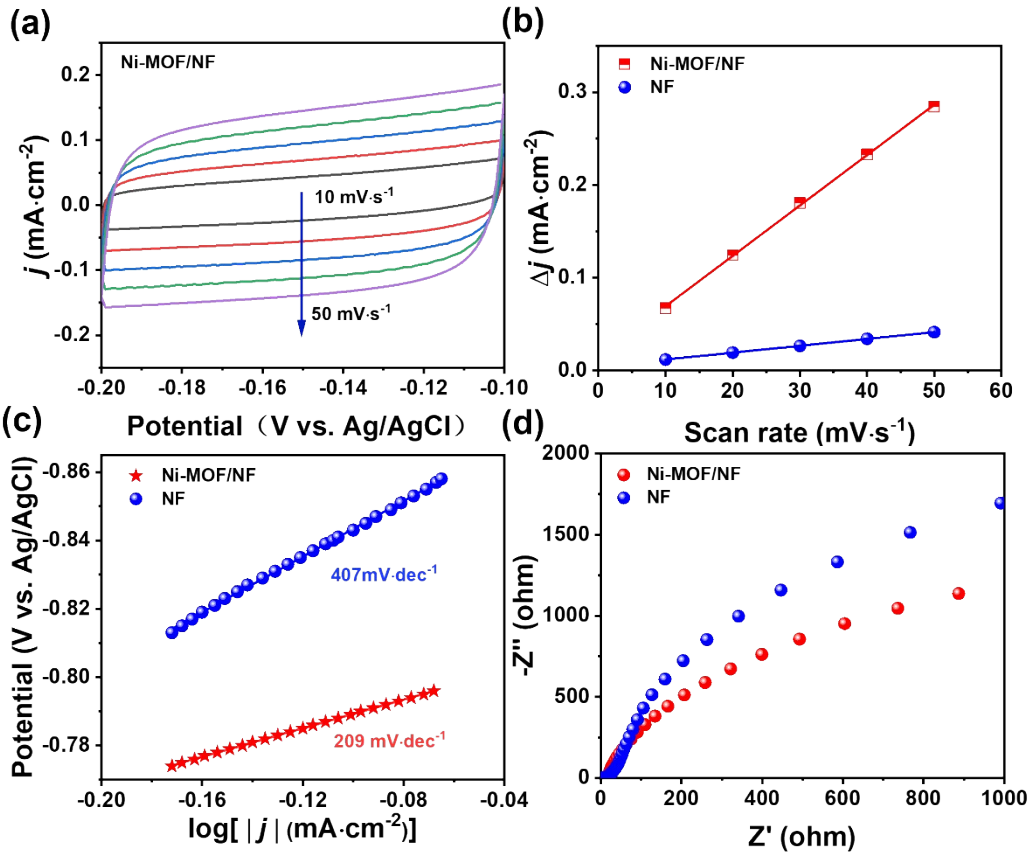

Fig. S17. (a) CV curves of Ni-MOF-400/NF at different scan rates. (b) Plots of current density differences vs. scan rates. (c) Tafel plots of Ni-MOF-400/NF and NF. (d) Nyquist plots of Ni-MOF-400/NF and NF. Measured condition: 0.1 M KOH, 0.5 Mm 4-NP.

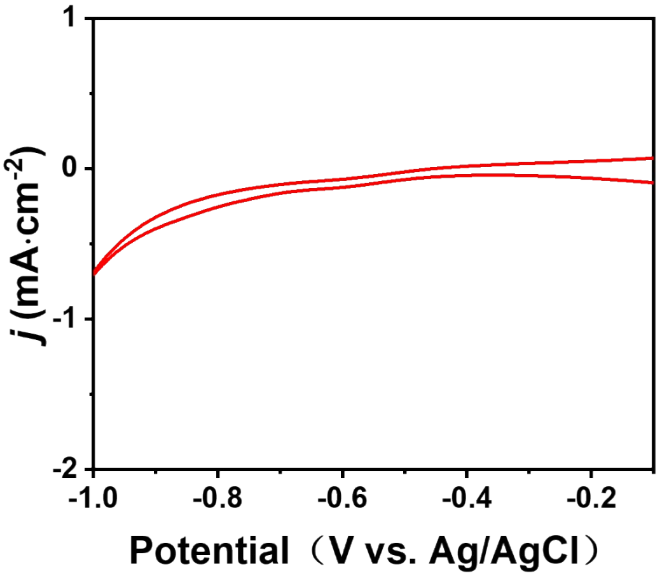

Fig. S18. CV curve of Ni-MOF/NF in 0.1 M KOH (without 4-NP).

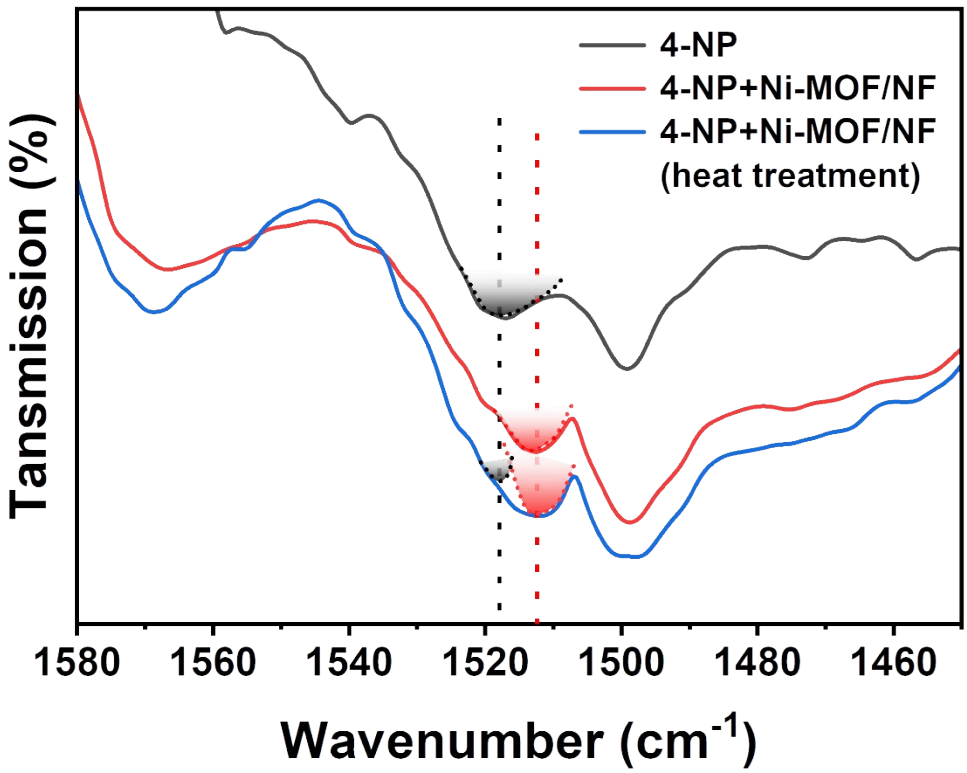

Fig. S19. FTIR spectroscopy of 4-NP, 4-NP+Ni-MOF and 4-NP+Ni-MOF (heat treatment), respectively.

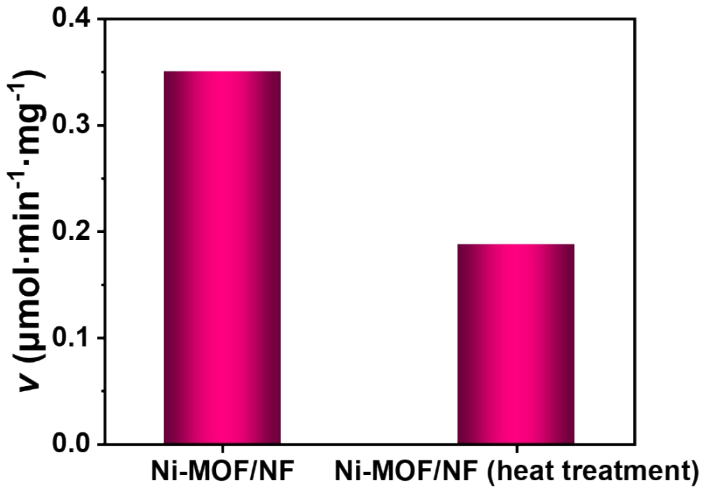

Fig. S20. Reaction rates of 4-NP for 2 h (-1.0 V vs. Ag/AgCl) over Ni-MOF-400/NF and Ni-MOF-400/NF (heat treatment).

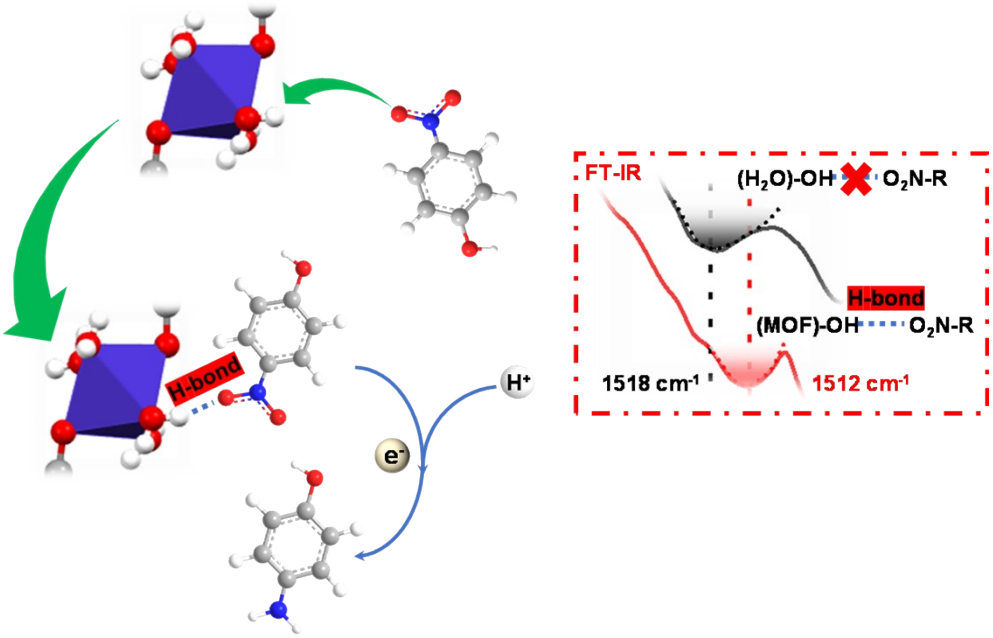

Fig. S21. Schematic diagram of 4-NP electrocatalytic reduction.

Table S1. Some recent work reports on the reduction of 4-NP

material	catalytic type	sacrificial agent	consumption of 4-NP (μmol)	Reaction rate ($\mu mol \cdot min^{-1} \cdot mg^{-1}$)	reference
Fe_3O_4/PPy-MAA/Ag	Thermal catalysis	$NaBH_4$	25	0.222	2
AuNS/pulp	Thermal catalysis	$NaBH_4$	4.92	0.030	3
Ag/Bi-$BiVO_4$	Thermal catalysis	$NaBH_4$	3.59	0.359	4
Ag/Pt/sepiolite	Thermal catalysis	$NaBH_4$	19.2	0.0128	5
Au NPs/CTS/AC	Thermal catalysis	$NaBH_4$	10	0.261	6
Au/Cu	Thermal catalysis	$NaBH_4$	1.71	0.0019	7
CDs/CuO/mHA	Photocatalysis	$NaBH_4$	2.16	0.018	8
CDs/$BiPO_4$	Photocatalysis	$NaBH_4$	1.35	0.016	9
Ni-MOF/NF	Electrocatalysis		22.8	0.161	This work

References

1. L. Wang, Y. Wu, R. Cao, L. Ren, M. Chen, X. Feng, J. Zhou and B. Wang, *ACS Appl. Mater. Interfaces*, 2016, **8**, 16736–16743.
2. R. Das, V. S. Sypu, H. K. Paumo, M. Bhaumik, V. Maharaj and A. Maity, *Appl. Catal. B*, 2019, **244**, 546–558.
3. Q. Jin, L. Ma, W. Zhou, Y. Shen, O. Fernandez-Delgado and X. Li, *Chem. Sci.*, 2020, **11**, 2915–2925.
4. M. Song, Y. Wu, C. Xu, X. Wang and Y. Su, *J. Hazard. Mater.*, 2019, **368**, 530–540.
5. Y. Ma, X. Wu and G. Zhang, *Appl. Catal. B*, 2017, **205**, 262–270.
6. Y. Fu, L. Qin, D. Huang, G. Zeng, C. Lai, B. Li, J. He, H. Yi, M. Zhang, M. Cheng and X. Wen, *Appl. Catal. B*, 2019, **255**, 117740.
7. R. Cai, P. R. Ellis, J. Yin, J. Liu, C. M. Brown, R. Griffin, G. Chang, D. Yang, J. Ren, K. Cooke, P. T. Bishop, W. Theis and R. E. Palmer, *Small*, 2018, **14**, 1703734.
8. Q. Chang, W. Xu, N. Li, C. Xue, Y. Wang, Y. Li, H. Wang, J. Yang and S. Hu, *Appl. Catal. B*, 2020, **263**, 118299.
9. Q. Chang, W. Yang, F. Li, C. Xue, H. Wang, N. Li, H. Liu, J. Yang and S. Hu, *Chem. Eng. J.*, 2020, **391**, 123551.